

Figure 5 Magnitude of measured and simulated S-parameters

operation of the resonator not only in azimuthally symmetric mode but also in azimuthally asymmetric modes. As is known, the diameter of ordinary cylindrical cavity resonators with dominant TM mode is equal to 0.7655λ . If we calculate the ratio of the diameter of the designed miniaturized cavity to the resonance wavelength of the TM_{010} mode of this cavity ($f_{TM_{010}} = 1.56$ GHz, see Fig. 5), it can be seen that the diameter of the cavity is only 0.31λ , which means that the diameter of the miniaturized cavity is shortened by 60%. It is worth to mention that using spiral resonator (SR) or multiple split-ring resonator (MSRR) type of inclusions [14] instead of BC-SRRs may result in a further miniaturization of the resonator due to the smaller size of these inclusions.

By varying F_1 , F_2 or the negative permeability bandwidth of the AMNG layer which can be adjusted using appropriate magnetic inclusions, it is possible to design a resonator with a distinct mode (as an example, TM_{010}) and to suppress the other modes.

4. CONCLUSIONS

In this letter, a coaxial miniaturized cylindrical cavity resonator is presented. The dispersion relations and their approximate forms have been derived for three different types of metamaterial fillings and it is shown that not only the azimuthally symmetric subwavelength resonance but also the azimuthally asymmetric subwavelength resonances can occur when the φ -direction permeability components ($\mu_{\varphi 1}$ and $\mu_{\varphi 2}$) have opposite sign. This simple criterion removes the need of realizing complex IDNG or IMNG media. Based on these results, a miniaturized coaxial cavity resonator partially filled with BC-SRR-based AMNG medium is designed, simulated, and fabricated. It is shown that the diameter of the miniaturized cavity is shortened by 60%.

REFERENCES

1. J. Garcia-Garcia, F. Martin, F. Falcone, J. Bonache, J.D. Baena, I. Gil, E. Amat, T. Lopetegui, M.A.G. Laso, J.A.M. Iturmendi, M. Sorolla, and R. Marques, Microwave filters with improved stop-band based on subwavelength resonators, *IEEE Trans Microwave Theory Tech* 53 (2005), 1997–2004.
2. A. Shelkovich and D. Budimir, Left-handed rectangular waveguide bandstop filters, *Microwave Opt Technol Lett* 48 (2006), 846–848.
3. R.W. Ziolkowski and A. Erentok, Metamaterial-based efficient electrically small antennas, *IEEE Trans Antennas Propag* 54 (2006), 2113–2130.

4. P. Jin and R.W. Ziolkowski, Broadband, efficient, electrically small metamaterial-inspired antennas facilitated by active near-field resonant parasitic elements, *IEEE Trans Antennas Propag* 58 (2010), 318–327.
5. M.A.Y. Abdalla, K. Phang, G.V. Eleftheriades, A planar electronically steerable patch array using tunable PRI/NRI phase shifters, *IEEE Trans Microwave Theory Tech* 58 (2009), 531–541.
6. N. Engheta, An idea for thin subwavelength cavity resonators using metamaterials with negative permittivity and permeability, *IEEE Antenna Wireless Propag Lett* 1 (2002), 10–13.
7. Y. Li, L. Ran, H. Chen, J. Huangfu, X. Zhang, K. Chen, T. Grzegorzczuk, and J.A. Kong, Experimental realization of a one-dimensional LHM-RHM resonator, *IEEE Trans Microwave Theory Tech* 53 (2005), 1522–1526.
8. S. Hrabar, J. Bartolic, and Z. Sipus, Experimental investigation of sub-wavelength resonator based on backward-wave meta-material, *IEEE Antennas Propag Soc Symp*, Monterey, CA (2004), 2568–2571.
9. T. Hand, S. Cummer, and N. Engheta, The measured electric field spatial distribution within a metamaterial subwavelength cavity resonator, *IEEE Trans Antennas Propag* 55 (2007), 1781–1788.
10. F.-Y. Meng, Q. Wu, and J.-H. Fu, Miniaturized rectangular cavity resonator based on anisotropic metamaterials bilayer, *Microwave Opt Technol Lett* 50 (2008), 2016–2020.
11. F.W.J. Olver, D.W. Lozier, and R.F. Boisvert, *NIST hand book of mathematical functions*, Cambridge University Press, Cambridge, England, 2010.
12. R. Marques, F. Medina, and R. Rafii-El-Idrissi, Role of bianisotropy in negative permeability and left-handed metamaterials, *Phys Rev B* 65 (2002), 144441–144446.
13. D.R. Smith, D.C. Vier, Th. Koschny, and C.M. Soukoulis, Electromagnetic parameter retrieval from inhomogeneous metamaterials, *Phys Rev E* 71 (2005), 0366171–03661711.
14. F. Bilotti, A. Toscano, and L. Vegni, Design of spiral and multiple split-ring resonators for the realization of miniaturized metamaterial samples, *IEEE Trans Antennas Propag* 55 (2007), 2258–2267.

© 2012 Wiley Periodicals, Inc.

INTERNAL COUPLED-FED LOOP ANTENNA INTEGRATED WITH NOTCHED GROUND PLANE FOR WIRELESS WIDE AREA NETWORK OPERATION IN THE MOBILE HANDSET

Fang-Hsien Chu and Kin-Lu Wong

Department of Electrical Engineering, National Sun Yat-Sen University, Kaohsiung 804, Taiwan; Corresponding author: wongkl@ema.ee.nsysu.edu.tw

Received 19 May 2011

ABSTRACT: An internal wireless wide area network (824–960/1710–2170 MHz) antenna suitable to be disposed at a notched region (size $10 \times 40 \text{ mm}^2$) of the system ground plane of the handset to achieve compact integration therein is presented. The notched system ground plane, compared to the traditional rectangular system ground plane at which the internal antenna is generally disposed at the entire top or bottom edge of the ground plane, can lead to more compact layout design of the internal antenna and associated electronic elements in the handset. The proposed antenna has a simple structure occupying a small volume of $10 \times 40 \times 5 \text{ mm}^3$ and comprising a monopole feed and a coupled strip. The latter is coupled-fed by the monopole feed to provide a 0.25-wavelength loop path, which generates a 0.25-wavelength loop mode at about 850 MHz and a higher-order loop mode at about 1.7 GHz. The monopole feed also contributes a 0.25-wavelength mode at about 2.1 GHz to combine with the higher-order loop mode to form the antenna's upper band. The bandwidth enhancement of the 0.25-wavelength loop mode is obtained by adding an external bandstop circuit, which makes the desired antenna's lower band achieved. The

Key words: mobile antennas; handset antennas; coupled-fed loop antennas; wireless wide area network antennas; notched system ground plane

1. INTRODUCTION

Traditional internal wireless wide area network (WWAN) antennas for the mobile handsets are mainly disposed at the entire top or bottom edge of the system ground plane. The reasons for the disposition of these internal WWAN antennas in the mobile handsets are mainly because these antennas are generally required to occupy a large volume to cover the desired wide operating bands of 824–960 and 1710–2170 MHz. Further, a certain isolation distance between these antennas and the nearby ground plane is usually required to achieve good radiation efficiency over a wide operating band for the antenna. Typical examples for such internal WWAN handset antennas that can cover the desired 824–960 and 1710–2170 MHz bands have been shown [1–9].

To closely integrate the antenna with nearby system ground plane on which the associated electronic elements can be accommodated, several related designs suitable for WWAN operations have been reported [10–18]. These reported antennas are suitable to be integrated with a protruded ground extended from the main ground plane (usually a simple rectangular ground plane) of the mobile handset. The protruded ground, which is large enough for mounting associated electronic elements such as a universal serial bus connector [10, 19], can be located at one corner [10–16] or at the center [17, 18] of one edge of the simple rectangular ground plane of the mobile handset. Further, it has been shown that the protruded ground can lead to decreased surface current distributions [12] on the

system ground plane away from the edge where the antenna is mounted. It is hence expected that by disposing the antenna at the bottom of the mobile handset, decreased near-field emission near the top portion or the acoustic output of the handset can be expected. This can make it promising for the handset to meet the specific absorption rate [SAR; 20, 21] and hearing-aid compatibility [HAC; 22–24] requirements for practical applications.

To further devise promising integration designs of the internal WWAN antenna with nearby ground planes, we present in this article an internal WWAN antenna suitable to be disposed at a notched region of the system ground plane of the handset to achieve compact integration therein. That is, the internal antenna is to closely integrate with two nearby protruded grounds extended at the two corners of the main ground plane of the handset, which is different from the case of only one nearby protruded ground for the internal WWAN antenna that have been studied [10–18]. Also, the two protruded grounds have a large size of $10 \times 10 \text{ mm}^2$ and both can be used to accommodate associated electronic elements as in the antenna designs studied in Refs. 10–18.

To fit in the notched region of the system ground plane with small or negligible coupling with the two nearby protruded grounds, the proposed antenna applies a coupled-fed loop structure comprising a monopole feed and a coupled strip. The latter is coupled-fed by the monopole feed to provide a 0.25-wavelength loop path, which generates a 0.25-wavelength loop mode [25–27] at about 850 MHz and a higher-order loop mode at about 1.7 GHz. The monopole feed also functions as a radiator [28] and contributes a 0.25-wavelength mode at about 2.1 GHz to combine with the higher-order loop mode to form the antenna's upper band to cover the 1710–2170 MHz band. As for obtaining a wide lower band for the antenna, the technique of using a three-element bandstop circuit [29] is applied, which results in a dual-resonance excitation of the 0.25-wavelength loop mode such that the desired antenna's lower band to cover the 824–960 MHz band is obtained. Detailed operating principle of the proposed antenna is described in this article. Results of the fabricated prototype of the proposed antenna are presented and discussed. Radiation characteristics of the antenna and its simulated SAR values for 1-g head tissue [20] and the HAC results for American National Standards Institute (ANSI) C63.10-2007 specification [22] are also shown.

2. PROPOSED ANTENNA

Figure 1(a) shows the geometry of the proposed coupled-fed loop antenna integrated with a notched system ground plane for WWAN operation in the mobile handset. Back view of the notched system ground plane is shown in Figure 1(b). Dimensions of the antenna's metal pattern are given in Figure 1(c). The configuration of the proposed antenna can be seen more clearly from the photos of the fabricated antenna shown in Figure 2. The notched region is at the bottom edge of the system circuit board of size $60 \times 115 \text{ mm}^2$, which is made by a 0.8-mm thick FR4 substrate of relative permittivity 4.4 and loss tangent 0.02 in this study. The selected dimensions of the system circuit board are reasonable for many commercially available smartphones. The notched region has a size of $10 \times 40 \text{ mm}^2$, and there are two protruded grounds of size $10 \times 10 \text{ mm}^2$ at both sides of the notched region. The two protruded grounds are connected to the main ground plane of size $60 \times 105 \text{ mm}^2$. Both the protruded grounds and the main ground plane are printed on the back side of the system circuit board and form the system ground plane of the mobile handset.

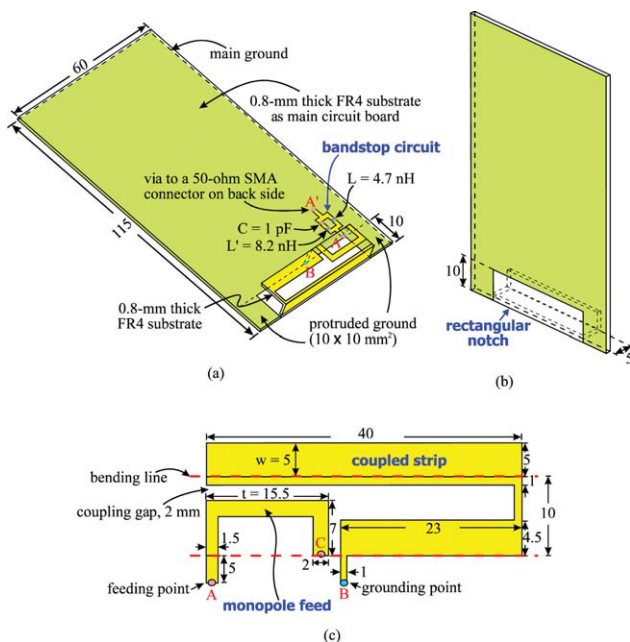


Figure 1 (a) Geometry of the proposed coupled-fed loop antenna integrated with a notched system ground plane for WWAN operation in the mobile handset. (b) Back view of the notched system ground plane. (c) Dimensions of the antenna's metal pattern. [Color figure can be viewed in the online issue, which is available at wileyonlinelibrary.com]

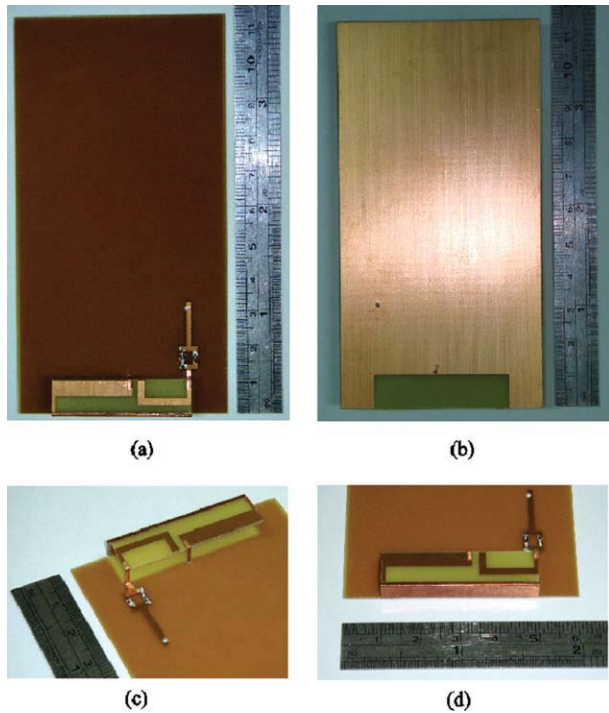


Figure 2 Photos of the fabricated antenna. (a) Front view. (b) Back view. (c) Front view seeing the feeding side of the antenna. (d) Front view seeing the widened open-end portion of the coupled strip. [Color figure can be viewed in the online issue, which is available at wileyonlinelibrary.com]

The antenna occupies a volume of $10 \times 40 \times 5 \text{ mm}^3$ and is disposed at the notched region. The antenna comprises a monopole feed and a coupled strip, and both are mainly printed on a 0.8-mm-thick FR4 substrate as shown in the figure. One end (Point A) of the monopole feed is the feeding point of the antenna. The monopole feed has a length of about 34.5 mm and can generate a 0.25-wavelength resonant mode at about 2.1 GHz. By tuning the length t in the monopole feed, the resonant mode generated by the monopole feed can be effectively controlled. Related results will be discussed in Section 4 with the aid of Figure 11.

Further, through a 2-mm coupling gap, the monopole feed couples to the coupled strip, whose one end (Point B) is grounded to the main ground plane, to provide a loop resonant

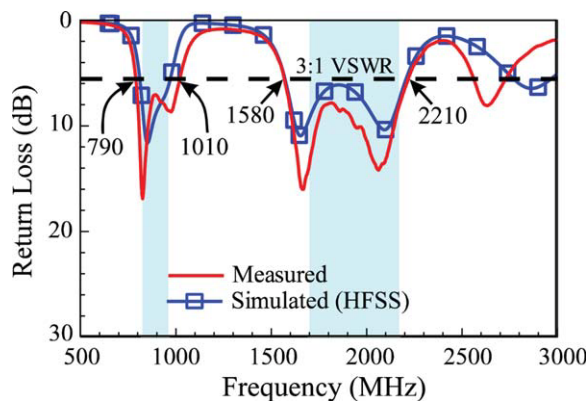
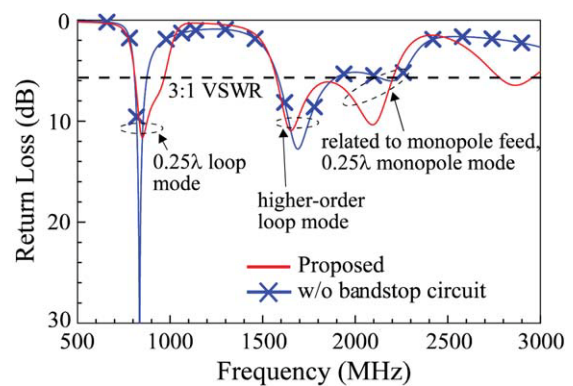


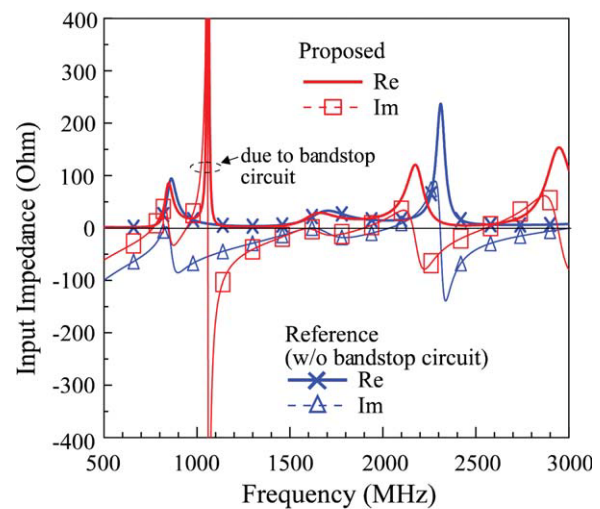
Figure 3 Measured and simulated return loss for the proposed antenna. [Color figure can be viewed in the online issue, which is available at wileyonlinelibrary.com]

path of about 97 mm, which is close to 0.25-wavelength at about 900 MHz. The loop resonant path can generate a 0.25-wavelength loop mode at about 900 MHz and a higher-order loop mode at about 1.7 GHz. The latter combines with the resonant mode generated by the monopole feed to form a wide operating band covering the GSM1800/1900/UMTS operation. As for the 0.25-wavelength loop mode, a dual-resonance excitation can be obtained by adding an external three-element bandstop circuit [29], which results in a wide operating band covering the GSM850/900 operation.

The reason for the dual-resonance excitation is because the bandstop circuit can generate a parallel resonance at about 1.1 GHz, which is slightly higher than the resonant frequency of the 0.25-wavelength loop mode. The parallel resonance can effectively compensate for the large capacitive reactance of the frequencies at the high-frequency tail of the 0.25-wavelength loop mode, thereby causing an additional resonance (zero reactance) occurred nearby the resonant frequency of the 0.25-wavelength loop mode. This condition leads to a dual-resonance excitation for the 0.25-wavelength loop mode. More detailed results are shown in Figure 4 and will be discussed in Section 3. Also, note that the coupled strip has a widened open-end section, which can shift the excited loop resonant modes to lower frequencies. By tuning the width w in the widened open-end section of the



(a)



(b)

Figure 4 Simulated (a) return loss and (b) input impedance for the proposed antenna and the case without the bandstop circuit. [Color figure can be viewed in the online issue, which is available at wileyonlinelibrary.com]

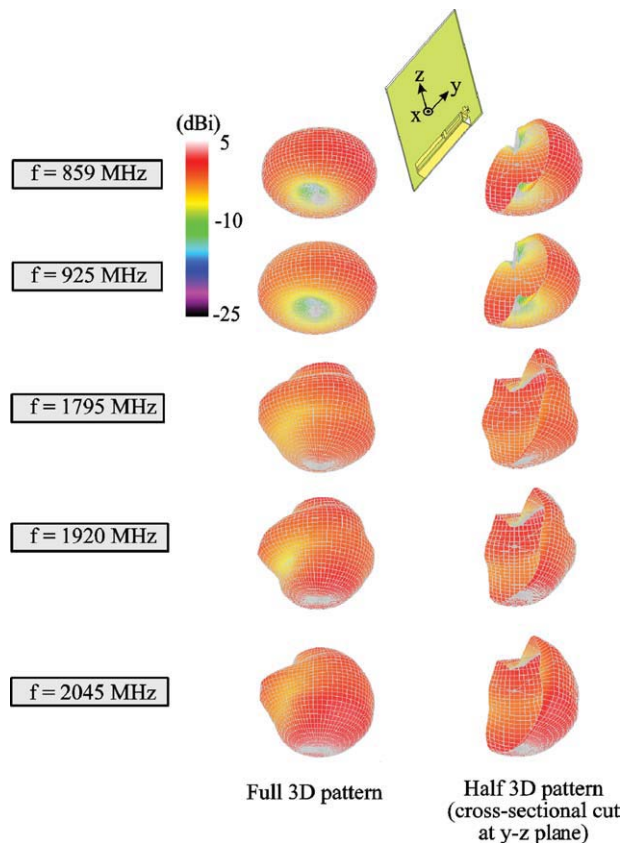


Figure 5 Measured 3D total-power radiation patterns for the proposed antenna. [Color figure can be viewed in the online issue, which is available at wileyonlinelibrary.com]

coupled strip, the excited loop resonant modes especially the 0.25-wavelength loop mode can be adjusted. Details of the results will be discussed in Section 4 with the aid of Figure 10.

3. RESULTS AND DISCUSSION

Figure 3 shows the measured and simulated return loss for the fabricated antenna. Simulated results are obtained using ANSYS simulation software high frequency structure simulator version 12 [30]. The measured data agree with the simulated results.

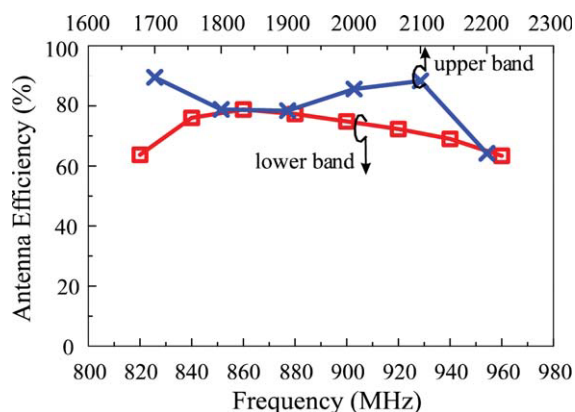
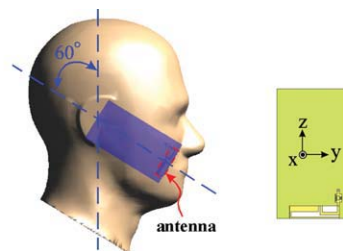


Figure 6 Measured antenna efficiency (mismatching loss included) for the proposed antenna. [Color figure can be viewed in the online issue, which is available at wileyonlinelibrary.com]

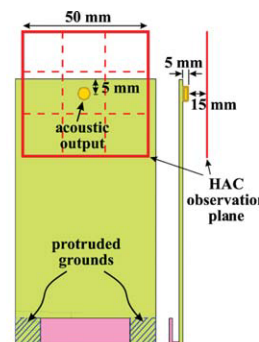


Frequency (MHz)	Testing power (dBm)	SAR (W/kg)	Return loss (dB)
859	24	0.89	14.6
925	24	0.88	10.6
1795	21	0.21	7.2
1920	21	0.20	7.5
2045	21	0.18	9.3

Figure 7 SAR simulation model and the simulated SAR values for 1-g head tissue for the proposed antenna. [Color figure can be viewed in the online issue, which is available at wileyonlinelibrary.com]

The obtained antenna's lower and upper bands, with impedance matching defined by 3:1 VSWR (6-dB return loss), cover the desired 824–960 and 1710–2170 MHz bands. Note that 3:1 VSWR is widely used as the design specification for the internal WWAN handset antenna.

To analyze the operating principle of the antenna, Figure 4 shows the simulated return loss and input impedance for the proposed antenna and the case without the bandstop circuit. In Figure 4(a), for the input impedance, it is seen that the bandwidth of the 0.25-wavelength loop mode without the bandstop circuit is much smaller than that of the proposed antenna. This



Frequency (MHz)		859	925	1795	1920	2045
Proposed	E-field (V/m in dB) (M3)	48.4	48.0	37.1	35.2	25.4
	H-field (A/m in dB) (M4)	-8.3	-8.1	-13.4	-13.8	-23.1
	Return Loss (dB)	11	9.9	7.2	7.6	9.6
w/o protruded grounds	E-field (V/m in dB) (M2)	48.8	48.8	43.0	41.4	31.2
	H-field (A/m in dB) (M4)	-7.9	-7.3	-8.8	-10.5	-20.5
	Return Loss (dB)	12.2	20.7	16.5	7.9	6.4
Testing power (dBm)		33	33	30	30	21

Figure 8 HAC simulation model and the simulated HAC results for the proposed antenna with the notched system ground plane and the case with a simple rectangular system ground plane (no protruded grounds). [Color figure can be viewed in the online issue, which is available at wileyonlinelibrary.com]

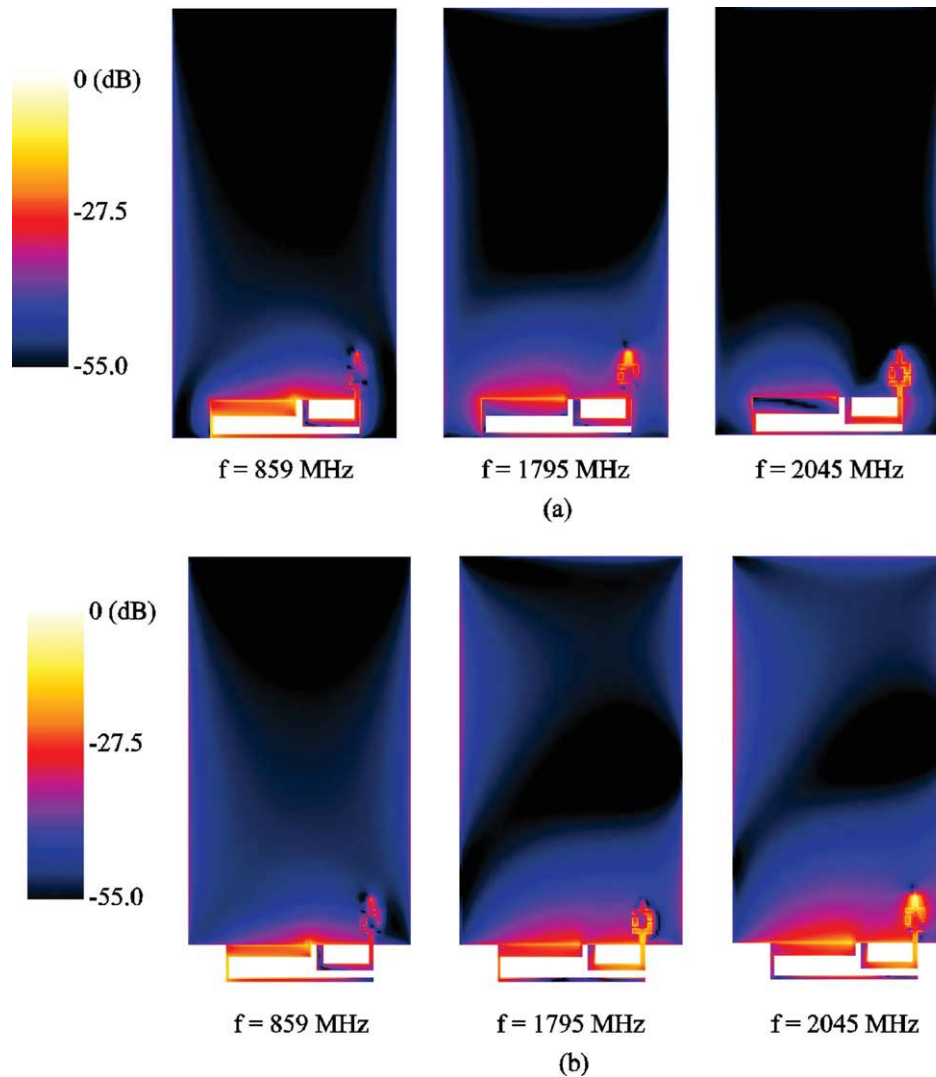


Figure 9 Simulated surface current distributions excited on (a) the notched system ground plane and (b) the simple rectangular system ground plane. The two ground planes are printed on the FR4 substrate of same dimensions ($115 \times 60 \text{ mm}^2$). [Color figure can be viewed in the online issue, which is available at wileyonlinelibrary.com]

behavior can be seen more clearly in Figure 4(b) for the input impedance. A parallel resonance is occurred at about 1.1 GHz at the high-frequency tail of the 0.25-wavelength loop mode. The parallel resonance especially improves the input reactance at frequencies around 900 MHz, resulting in an additional resonance (zero reactance) occurred at about 950 MHz. This additional resonance leads to a dual-resonance excitation of the 0.25-wavelength loop mode, and hence a wide antenna's lower band is obtained. The bandstop circuit also improves the impedance matching for the 0.25-wavelength mode of the monopole feed, leading to better return loss obtained for frequencies in the desired antenna's upper band.

The measured three-dimensional (3D) total-power radiation patterns are plotted in Figure 5. The antenna is tested in a far-field anechoic chamber. The full 3D patterns and half 3D patterns with the cross-sectional cut at the y - z plane are shown. Results at five typical frequencies of 859, 925, 1795, 1920, and 2045 MHz are presented. At lower frequencies of 859 and 925 MHz, dipole-like radiation patterns with omnidirectional radiation in the azimuthal plane (x - y plane) are observed. At higher frequencies of 1795, 1920, and 2045 MHz, some dips near the azimuthal plane of the radiation pat-

terns are seen, which is related to the surface current nulls on the main ground plane of the handset at higher frequencies. Figure 6 presents the measured antenna efficiency of the fabricated antenna. The antenna efficiency includes the mismatching loss of the antenna. The antenna efficiency varies in the range of about 63–78% and 63–90% for frequencies over the lower and upper bands, respectively. The results indicate that good radiation characteristics are obtained for the proposed antenna.

Figure 7 shows the SAR simulation model and the simulated SAR values for 1-g head tissue. The simulation model is based on the simulation software SEMCAD X version 14 [31]. The simulated SAR values obtained at typical frequencies of the five operating bands are listed in the table in the figure. The return loss showing the impedance matching level at each testing frequency is also given. The input power for the SAR testing is 24 dBm or 0.25 W for the GSM850/900 operation (859 and 925 MHz) and 21 dBm or 0.125 W for the GSM1800/1900/UMTS operation (1795, 1920, and 2045 MHz). The obtained SAR values for 1-g head tissue are well below the limit of 1.6 W/kg, indicating that the proposed antenna is promising for practical handset applications.

Figure 8 shows the HAC simulation model and the simulated HAC results for the proposed antenna with the notched system ground plane and the case with a simple rectangular system ground plane (no protruded grounds). The HAC model is based on the standard ANSI C63.19-2007 [22] and provided by SEMCAD X version 14 [31]. The HAC testing power is 33 dBm (2 W continuous input power) for the GSM850/900 operation (859 and 925 MHz), 30 dBm (1 W continuous input power) for the GSM1800/1900 operation (1795 and 1920 MHz), and 21 dBm (0.125 W continuous input power) for the UMTS operation (2045 MHz). The return loss at each testing frequency is also given in the figure. The HAC results are obtained at the observation plane of $50 \times 50 \text{ mm}^2$ centered above the acoustic output center with a height of 15 mm. The obtained near-field E-field and H-field strengths for the HAC testing are seen to be rated in the M3 or M4 category [22–24], indicating that the proposed antenna with the notched system ground plane can lead to a hearing-aid compatible mobile handset (the HAC results should all be in the M3 or higher category). Also, the obtained E-field and H-field strengths are weaker for the proposed antenna with the notched system ground plane than for the corresponding case with a simple rectangular system ground plane (for example, at 1920 MHz, the E-field and H-field for the proposed case are weaker by about 6.2 and 3.3 dB, respectively, than those for the case without protruded grounds). Also, note that the latter is rated in the M2 category and cannot be treated to be an HAC mobile handset.

The improvements in the HAC behavior can be seen more clearly from the simulated surface current distributions excited on the notched system ground plane and the simple rectangular system ground plane as shown in Figure 9. It can be seen that the protruded grounds can attract some excited surface currents such that those on the main ground plane are decreased for the notched system ground plane. In this case, decreased near-field emission observed at the HAC observation plane can be expected.

4. PARAMETRIC STUDY

Effects of some design parameters are also studied. Figure 10 shows the simulated return loss as a function of the width w in the widened open-end section of the coupled strip. Other dimensions are the same as in Figure 1. Results for the width w varied from 3 to 5 mm are shown in Figure 10. It is seen that the two

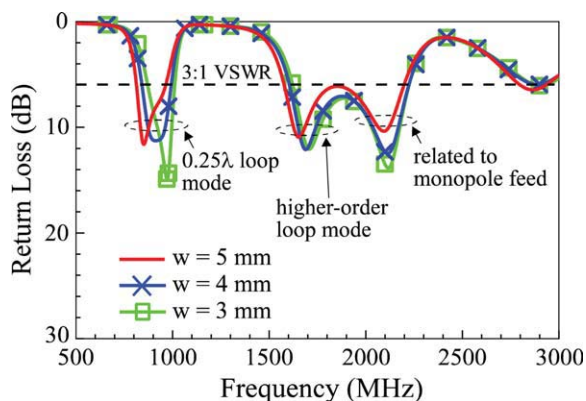


Figure 10 Simulated return loss as a function of the width w in the widened open-end section of the coupled strip. Other dimensions are the same as in Figure 1. [Color figure can be viewed in the online issue, which is available at wileyonlinelibrary.com]

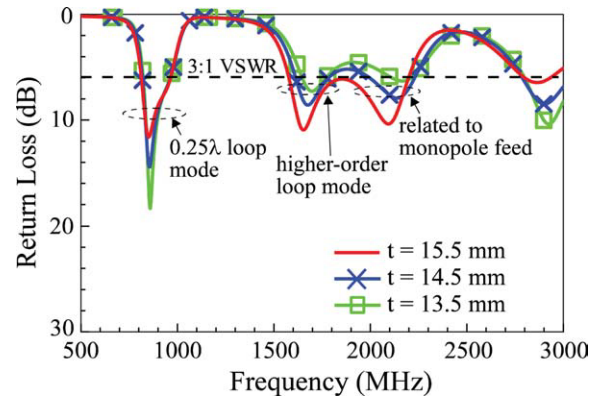


Figure 11 Simulated return loss as a function of the length t in the monopole feed. Other dimensions are the same as in Figure 1. [Color figure can be viewed in the online issue, which is available at wileyonlinelibrary.com]

loop modes at about 900 and 1700 MHz are shifted to lower frequencies with an increase in the width w . As the coupled strip is a major portion of the loop path provided in the proposed antenna, it is reasonable that a larger width w in the coupled strip can lead to an increase in the resonant length of the loop path, which decreases the resonant frequency of the excited loop modes. As for the resonant mode at about 2.1 GHz, only the impedance matching is affected by the variations in the width w , and the resonant frequency is generally not affected.

Figure 11 shows the simulated return loss as a function of the length t in the monopole feed. Results for the length t varied from about 13.5 to 15.5 mm are shown. Relatively large effects on the resonant mode related to the monopole feed are seen, indicating that the resonant mode at about 2.1 GHz can be controlled by adjusting the length t . For the 0.25-wavelength loop mode at about 900 MHz, only the impedance matching level is affected. This is reasonable, as the variations in the length t will lead to some effects in the coupling excitation of the loop resonant mode. Compared with the 0.25-wavelength loop mode, the observed effects on the loop mode at about 1.7 GHz are larger, which is probably because it is a higher-order loop mode, and a current null (that is, strong electric field) will occur in the coupled strip [32]. In this case, the coupling variations between the monopole feed and the coupled strip will lead to larger effects on the higher-order loop mode than on the fundamental 0.25-wavelength loop mode.

5. CONCLUSIONS

An internal penta-band WWAN antenna especially suitable to be applied in the handset having a notched system ground plane has been proposed and studied. The use of an external bandstop circuit, which does not increase the antenna volume, to enhance the lower-band bandwidth of the antenna has been demonstrated. Detailed operating principle of the proposed antenna has also been studied. The fabricated prototype of the proposed antenna showed two wide operating bands with good radiation characteristics for the penta-band WWAN operation. With the notched system ground plane, the proposed antenna also showed decreased near-field emissions such that the antenna can meet the SAR and HAC requirements. The results make the proposed antenna with the notched system ground plane very promising for practical handset applications.

REFERENCES

1. A. Cabedo, J. Anguera, C. Picher, M. Ribo, and C. Puente, Multi-band handset antenna combining a PIFA, slots, and ground plane modes, *IEEE Trans Antennas Propag* 57 (2009), 2526–2533.
2. K.L. Wong and L.C. Lee, Multiband printed monopole slot antenna for WWAN operation in the laptop computer, *IEEE Trans Antennas Propag* 57 (2009), 324–330.
3. H. Rhyu, J. Byun, F.J. Harackiewicz, M.J. Park, K. Jung, D. Kim, N. Kim, T. Kim, and B. Lee, Multi-band hybrid antenna for ultrathin mobile phone applications, *Electron Lett* 45 (2009), 773–774.
4. C.H. Chang and K.L. Wong, Printed $\lambda/8$ -PIFA for penta-band WWAN operation in the mobile phone, *IEEE Trans Antennas Propag* 57 (2009), 1373–1381.
5. K.L. Wong and S.C. Chen, Printed single-strip monopole using a chip inductor for penta-band WWAN operation in the mobile phone, *IEEE Trans Antennas Propag* 58 (2010), 1011–1014.
6. C.L. Liu, Y.F. Lin, C.M. Liang, S.C. Pan, and H.M. Chen, Miniature internal penta-band monopole antenna for mobile phones, *IEEE Trans Antennas Propag* 58 (2010), 1008–1011.
7. M.R. Hsu and K.L. Wong, Seven-band folded-loop chip antenna for WWAN/WLAN/WiMAX operation in the mobile phone, *Microwave Opt Technol Lett* 51 (2009), 543–549.
8. T.W. Kang and K.L. Wong, Chip-inductor-embedded small-size printed strip monopole for WWAN operation in the mobile phone, *Microwave Opt Technol Lett* 51 (2009), 966–971.
9. J.Y. Sze and Y.F. Wu, A compact planar hexa-band internal antenna for mobile phone, *Prog Electromagn Res* 107 (2010), 413–425.
10. K.L. Wong, M.F. Tu, C.Y. Wu, and W.Y. Li, On-board 7-band WWAN/LTE antenna with small size and compact integration with nearby ground plane in the mobile phone, *Microwave Opt Technol Lett* 52 (2010), 2847–2853.
11. S.C. Chen and K.L. Wong, Bandwidth enhancement of coupled-fed on-board printed PIFA using bypass radiating strip for eight-band LTE/GSM/UMTS slim mobile phone, *Microwave Opt Technol Lett* 52 (2010), 2059–2065.
12. S.C. Chen and K.L. Wong, Hearing aid-compatible internal LTE/WWAN bar-type mobile phone antenna, *Microwave Opt Technol Lett* 53 (2011), 774–781.
13. S.C. Chen and K.L. Wong, Planar strip monopole with a chip-capacitor-loaded loop radiating feed for LTE/WWAN slim mobile phone, *Microwave Opt Technol Lett* 53 (2011), 952–958.
14. K.L. Wong and Y.W. Chang, Internal eight-band WWAN/LTE handset antenna using loop shorting strip and chip-capacitor-loaded feeding strip for bandwidth enhancement, *Microwave Opt Technol Lett* 53 (2011), 1217–1222.
15. F.H. Chu and K.L. Wong, On-board small-size printed LTE/WWAN mobile handset antenna closely integrated with nearby system ground plane, *Microwave Opt Technol Lett* 53 (2011), 1336–1343.
16. K.L. Wong, T.W. Kang, and M.F. Tu, Antenna array for LTE/WWAN and LTE MIMO operations in the mobile phone, *Microwave Opt Technol Lett* 53 (2011), 1569–1573.
17. K.L. Wong, W.Y. Chen, and T.W. Kang, On-board printed coupled-fed loop antenna in close proximity to the surrounding ground plane for penta-band WWAN mobile phone, *IEEE Trans Antennas Propag* 59 (2011), 751–757.
18. K.L. Wong and C.H. Chang, On-board small-size printed monopole antenna integrated with USB connector for penta-band WWAN mobile phone, *Microwave Opt Technol Lett* 52 (2010), 2523–2527.
19. Universal Serial Bus (USB), Available at: <http://www.usb.org/>.
20. American National Standards Institute (ANSI), Safety levels with respect to human exposure to radio-frequency electromagnetic field, 3 kHz to 300 GHz, ANSI/IEEE standard C95.1, April 1999.
21. IEC 62209-1, Human exposure to radio frequency fields from hand-held and body-mounted wireless communication devices—Human models, instrumentation, and procedures—Part 1: Procedure to determine the specific absorption rate (SAR) for hand-held devices used in close proximity to the ear (frequency range of 300 MHz to 3 GHz), February 2005.
22. American national standard for method of measurement of compatibility between wireless communication devices and hearing aids (ANSI C63.19-2007, revision ANSI C63.19-2006), American National Standards Institute, New York, 2007.
23. K.L. Wong and M.F. Tu, Hearing aid-compatible internal penta-band antenna for clamshell mobile phone, *Microwave Opt Technol Lett* 51 (2009), 1408–1413.
24. T. Yang, W.A. Davis, W.L. Stutzman, and M.C. Huynh, Cellular-phone and hearing-aid interaction: An antenna solution, *IEEE Antennas Propag Mag* 50 (2008), 51–65.
25. Y.W. Chi and K.L. Wong, Quarter-wavelength printed loop antenna with an internal printed matching circuit for GSM/DCS/PCS/UMTS operation in the mobile phone, *IEEE Trans Antennas Propag* 57 (2009), 2541–2547.
26. Y.W. Chi and K.L. Wong, Very-small-size printed loop antenna for GSM/DCS/PCS/UMTS operation in the mobile phone, *Microwave Opt Technol Lett* 51 (2009), 184–192.
27. K.L. Wong and W.Y. Chen, Small-size printed loop antenna for penta-band thin-profile mobile phone application, *Microwave Opt Technol Lett* 51 (2009), 1512–1517.
28. T.W. Kang, K.L. Wong, L.C. Chou, and M.R. Hsu, Coupled-fed shorted monopole with a radiating feed structure for eight-band LTE/WWAN operation in the laptop computer, *IEEE Trans Antennas Propag* 59 (2011), 674–679.
29. Y.W. Chi and K.L. Wong, Very-small-size folded loop antenna with a band-stop matching circuit for WWAN operation in the mobile phone, *Microwave Opt Technol Lett* 51 (2009), 808–814.
30. ANSYS HFSS, Available at: <http://www.ansys.com/products/hf/hfss/>.
31. SPEAG SEMCAD, Schmid and Partner Engineering AG, Available at: <http://www.semcad.com>.
32. Y.W. Chi and K.L. Wong, Compact multiband folded loop chip antenna for small-size mobile phone, *IEEE Trans Antennas Propag* 56 (2008), 3797–3803.

© 2012 Wiley Periodicals, Inc.

A 0.18- μ M SiGe BiCMOS HBT VCO USING DIODE DEGENERATION

Sheng-Lyang Jang, Chao-Wei Hsieh, Chia-Wei Chang, and Ching-Wen Hsue

Department of Electronic Engineering, National Taiwan University of Science and Technology, No. 43, Sec. 4, Keelung Road, Taipei106, Taiwan, Republic of China; Corresponding author: sljij@mail.ntust.edu.tw

Received 19 May 2011

ABSTRACT: This letter proposes a BiCMOS voltage-controlled oscillator (VCO), which was implemented in the standard TSMC 0.18 μ m SiGe 3P6M BiCMOS process. The VCO consists of an nMOSFET cross-coupled oscillator stacked in series with source degenerated HBT diodes. SiGe HBT has an inherently low flicker noise compared to CMOS devices. At the supply voltage of 1.5 V, the output phase noise of the VCO is -122.01 dBc/Hz at 1 MHz offset frequency from the carrier frequency of 5.6 GHz, and the figure of merit is -190.43 dBc/Hz.

© 2012 Wiley Periodicals, Inc. *Microwave Opt Technol Lett* 54:605–608, 2012; View this article online at wileyonlinelibrary.com. DOI 10.1002/mop.26619

Key words: LC cross-coupled voltage-controlled oscillators; SiGe HBT; source degeneration

1. INTRODUCTION

Being a key block of monolithic wireless transceivers, fully integrated LC-tank voltage controlled oscillators (VCOs) are of great interest. SiGe BiCMOS has become a dominant